PAPER TO BE PRESENTED TO THE VI INTERNATIONAL CONFERENCE ON

HIGH-ENERGY ACCELERATORS

CAMBRIDGE, Mass.

U.S.A.

A GENERAL THEORY OF MULTISTEM DRIFT TUBE STRUCTURES PROPOSED FOR

PROTON LINACS

by

G. Dôme and I. White

CERN

Geneva, Switzerland, 6 September, 1967

1. INTRODUCTION

Conventional Alvarez proton linacs are operated at the zero-mode cut-off frequency of the E_{01} standing wave in a drift-tube loaded circular tank. The frequency difference between the operating mode and the adjacent mode is small, making the Alvarez structure rather sensitive to individual cell tuning errors [1] and beam-loading compensation [2].

Great advantage could thus be gained by increasing as much as possible the mode spacing around the operating E_{010} mode. This means modifying the dispersion curve of the E_{01} passband, which is possible only if this passband is coupled to another passband, the position of which could be largely varied with respect to the E_{01} passband [3]. It should be noticed that this principle was discovered in 1956 by the Harwell team [4].

The work undertaken in the Rutherford High Energy Laboratory and later on in CERN, on the cross-bar structure, had shown the existence of a lower passband, of the backward wave type, due to the bar resonances. The 0-mode cut-off frequency ω_b of this lower passband rises continuously with increasing bar diameter, whereas the E_{010} cut-off frequency ω_a remains practically unchanged [5]. An interesting situation arises when $\omega_b = \omega_a$: for this particular bar diameter, the two passbands (bar and E_{01}) cross each other at 0-mode with a finite slope, thereby producing large mode spacing near this point. In fact, this is the only case where the two dispersion curves cross each other: if the bar diameter is further increased, the 0-mode of the lower passband stays unchanged at the frequency ω_a of the Alvarez field configuration, while the upper passband starts still higher in frequency (see fig. 1). A new stopband arises, and the mode spacing around the Alvarez operating point decreases, due now to the adjacent mode in the lower passband. The largest mode spacing is thus obtained when the two passbands cross at 0-mode.

An important remark should be made about the field configurations which correspond to ω_a and ω_b : ω_a is the frequency of an Alvarez field configuration, i.e. a loaded E_{010} type of field. As such, it is only slightly perturbed by the bars irrespective of their diameter, because the bars are perpendicular to the electric field in this configuration and they do not carry any net longitudinal current. On the other hand, ω_b is the zero-mode frequency of the bar resonances, which are associated with currents flowing along the bars, all currents being equal in amplitude and phase throughout the structure. If, as usual, the cavity is terminated by a metallic end-plate placed in a cell symmetry plane, the boundary conditions require that, in 0-mode, these currents be zero in all bars. The corresponding fields are therefore zero everywhere, making it impossible to excite this field con-

figuration and to directly measure ω_b in a cavity of finite length. It is thus clear that, when $\omega_b = \omega_a$, the only field configuration which can be excited in a practical cavity at this frequency is the Alvarez type of field, and this conclusion has been confirmed in all our measurements.

We have explained how, for the cross-bar structure, crossing of the two passbands can be achieved by increasing the bar diameter to a suitable value. In the Alvarez structures which have been built up to now, each drift tube is supported by one stem, or eventually by two stems at 90°. The resonances of these drift-tube terminated stems constitute a second passband, similar to the cross-bar passband, but which lies in general well below the normal E_{01} passband. It was Giordano's idea to push this lower passband up in frequency by increasing the number of stems [6], thereby producing what he called a multistem structure. On his 100 MeV proton linac model, Giordano found that 4 flared stems were needed to get the E_{01} and the stem-passband crossing each other at 0-mode. In fact, Giordano's early measurements [7] stimulated at CERN an attempt to produce a theory which would give the conditions for stopband elimination in the case of a more general stem arrangement than the cross-bar structure. This general theory will now be presented.

2. THE CASE OF INFINITELY SHORT CELLS

a) One stem per drift tube. In order to produce the ω_b field configuration, we must imagine an infinitely long cavity where all bars carry identical currents and all drift tubes are charged with identical electric charges (see fig. 2a). In this case there is little field in the gaps between the drift tubes, and we do not alter the frequency very much if we fill in the gaps with metal, thus obtaining the arrangement of fig. 2b where a coaxial inner conductor having the same diameter d as the drift tubes is periodically supported by the stems. Now, if the distance L between adjacent stems is very small compared with the cavity diameter, the stems may be replaced by a thin partition wall extending between the inner and outer cylinders, as in fig. 2c. Finally we have transformed our initial structure into a uniform cylindrical coaxial waveguide with a partition wall representing the stems.

In order to produce the ω_b field configuration, the currents on both sides of the partition wall must flow in the same direction and this direction must be radial. Therefore, the uniform waveguide mode which represents the ω_b field configuration is an H_ν mode at cut-off, with H_z varying as $\cos \nu\varphi$ (see fig. 2d). Since H_z must change sign on both sides of the partition wall, ν must be a half-integer and the lowest mode corresponds to $\nu = 1/2$. Therefore, in the case of one stem per drift tube and very short cells, a good approximation to ω_b is given by the frequency of the $H_{\frac{1}{2}10}$ first mode in the equivalent uniform coaxial waveguide. Let us remark in passing that this equivalence only applies at 0-mode.

The current distribution along the stems is given by the radial variation of H_z, i.e. by Bessel functions of order ν and argument kr. For the first $H_{\nu 1}$ mode, H_z has no zero between the inner and outer cylinders, and therefore the current keeps a constant sign along the stems.

b) Two stems per drift tube. The two stems define two angles: one is smaller, the other larger than π. Let us call $\emptyset$ the latter one. Reasoning as before, we see that for very short cells a good approximation to ω_b is given by the frequency of the $H_{\nu 10}$ mode in the equivalent uniform coaxial waveguide with two partition walls at an angle $\emptyset$ (see fig. 3). Two cases are possible, according to whether the currents in the two stems have the same (fig. 3a) or have opposite (fig. 3b) radial signs: in the first case $\nu\emptyset/\pi$ must be an odd integer, in the second case it must be an even integer.

Figure 4 shows a graph of $\omega D/2c$ for the $H_{\nu 10}$ mode as a function of d/D, with ν as parameter. When $\nu > 0$ this mode is the dominant mode (mode with the lowest cut-off frequency) in the coaxial partitioned waveguide: it corresponds to an azimuthal resonance, by contrast with all the upper modes which correspond to radial resonances, where H_z undergoes at least one change of sign between the inner and outer cylinders. For $\nu = 0$ there is no azimuthal resonance possible, and the lower mode already corresponds to a radial resonance which is much higher in frequency ($\omega D/2c$ is at least 3.832). Disregarding therefore the case $\nu = 0$, we see on figure 4 that $\omega D/2c$ is an ever increasing function of ν.

Since ω_b is the cut-off frequency of the lowest passband, it must be as low a frequency as possible. Therefore, for a given $\emptyset$, it corresponds to the lowest value of $\nu\emptyset/\pi$, that is $\nu\emptyset/\pi = 1$ (see fig. 3a). The possibility of the radial currents having opposite signs (fig. 3b), since it corresponds to higher values of $\nu\emptyset/\pi$, needs no further consideration.

It is thus easy to vary ν and ω_b by varying the angle $\emptyset$ between the stems, a larger angle producing a lower frequency. Since two angles are defined by the two stems, it might be expected that two 0-mode frequencies and therefore two passbands are associated with stem resonances such that $\nu \, \emptyset/\pi = 1$. So far we have not found any experimental evidence for a higher stem-passband of this type. There-fore, only the lowest frequency, determined by the largest angle between stems, will be considered in what follows: this is the reason why we take $\emptyset \geqslant \pi$. Consequently, a two-stem structure allows the range $1/2 \leqslant \nu \leqslant 1$ to be covered. The maximum value $\nu = 1$ is obtained with two stems equally spaced at 180°.

c) Three stems per drift tube. Since only the largest angle $\emptyset$ defined by the stems is relevant, we do not change ω_b by taking the two smaller angles as equal : this gives the symmetrical arrangement of figure 5a. It is obvious from this figure that $\emptyset$ may be varied from 2π to $2\pi/3$. The range $2\pi \geqslant \emptyset \geqslant \pi$ being already covered with two stems per drift tube, the range $\pi \geqslant \emptyset \geqslant 2\pi/3$ is typical of a three-stem structure : it can also be achieved with the symmetrical arrangement of figure 5b.

Therefore, a three-stem structure allows the range $1/2 \leqslant \nu \leqslant 3/2$ to be covered. The maximum value $\nu = 3/2$ is obtained with the stems equally spaced at 120°.

d) Four stems per drift tube. Calling always $\emptyset$ the largest angle defined by the stems, we may assume that $\emptyset \leqslant \pi$ (the larger values of $\emptyset$ may be obtained with two stems). We do not change ω_b if we take the second large angle as equal to $\emptyset$, and divide the remaining angle in two equal parts $(\pi-\emptyset)$: this gives the symmetrical arrangement of figure 6a, which may be transformed into the even more symmetrical arrangement of figure 6b. It is clear that $\emptyset$ may be varied from π to $\pi/2$.

Consequently, a four-stem structure allows the range $1/2 \leqslant \nu \leqslant 2$ to be covered. The maximum value $\nu = 2$ is obtained with the stems equally spaced at 90°.

More generally, a N-stem structure allows the range $1/2 \leqslant \nu \leqslant N/2$ to be covered. The maximum value $\nu = N/2$ is obtained with equally spaced stems.

3. THE CASE OF FINITE CELL LENGTH L.

Strictly speaking, the above results only apply to infinitely short cells and, because $d_s/L \leqslant 1$, also to infinitely thin stems. When L is finite, it may be expected that, if thick enough, the stems will still be equivalent to a continuous partition wall at 0-mode. In fact, the effect of stem diameter may be investigated by considering (see fig. 2b) a stem as the inner conductor of a trans-mission line, the outer "conductor" being constituted by the cavity walls assumed to be at a constant distance $D/2$, and by two magnetic walls at a distance $L/2$ (see fig. 7). The characteristic impedance of such a line is readily obtained as

$$Z_o \approx \frac{1}{2\pi}\sqrt{\frac{\mu_o}{\varepsilon_o}} \quad \left[\frac{\pi}{2}\,\frac{D}{L} - \log\left(\pi\,\frac{d_s}{L}\right)\right] \qquad \frac{L}{D} < 1$$

This line is short-circuited at one end by the cavity wall, and terminated at the other end by the drift tube capacitance C, which may be approximated as $C_1 L$ where C_1 is the capacitance per unit length of the central pipe in figure 2b. In case of one or two stems per drift tube, the 0-mode stem resonance is thus roughly given by

$$k \cdot tg\,\frac{kD}{2} = \frac{1}{C\,cZ_o} = \frac{\sqrt{\varepsilon_o\,\mu_o}}{C_1 L\,Z_o} \qquad k = \frac{\omega_b}{c}$$

or

$$\frac{kD}{2}\cdot tg\,\frac{dD}{2} = \frac{\pi\,\varepsilon_o}{C_1\left[\frac{\pi}{2}-\frac{L}{D}\log\left(\pi\,\frac{d_s}{L}\right)\right]} \qquad C_1 \neq 0$$

Detailed calculations on the cross-bar and the 4-stem structures [8] replace this equation by the more general one

$$f\left[(kD)^2\right] = \frac{L}{D}\log\left(\pi\,\frac{d_s}{L}\right) \qquad \frac{L}{D} \ll 1 \qquad (1)$$

where f is an ever increasing function of its argument, but different

for each stem configuration.

The general relation (1) yields two important results:

1) ω_b is an ever increasing function of d_s .

2) the same ω_b is obtained for $\frac{L}{D} = 0$ and for $\pi\,\frac{d_s}{L} = 1$.

This result is obviously approximate because equation (1) only holds when $L/D \ll 1$.

By increasing $\pi\,d_s/L$ from 0 to 1 , it is thus possible to raise ω_b continuously from zero (for a structure with drift-tubes) to the limit obtained for infinitely short cells.

Conclusion: For a finite cell length, the frequency ω plotted in figure 4 is an upper limit of ω_b , which can be reached only with thick stems (such that $\pi\,d_s/L \approx 1$).

4. THE USE OF A SUPERPERIOD pL.

In order that the arguments of § 2 for infinitely short cells to be valid, it is not necessary that every drift tube is supported by N stems, giving the structure a period L along the z-axis. Instead, the structure may have a period $p L$ ($p = 1, 2, 3...$) involving less than N stems per drift-tube, under the condition that the cross-sectional projections of all stems contained in a superperiod would yield a N-stem pattern, like those in figures 3, 5 and 6. All these structures have the same frequency limit ω_b for infinitely short cells, as plotted in figure 4 : but in order to reach this limit with finite cells, they will need stems about p times as thick (such that $\pi\,d_s/pL \approx 1$) as a N-stem structure with period L . If used with the same stem diameter, they will have a lower ω_b than the latter : in other words, they are less efficient in raising ω_b .

Nevertheless, for a given number n of stems on each drift tube, the stem arrangement in a superperiod pL ($p > 1$) yielding a N-stem pattern ($N > n$) will be more efficient than the normal n-stem pattern with period L . Even if both structures have the same stem diameter, this argument still applies because the ω_b - upper limit strongly increases with N (see fig. 4) although the variation of ω_b with d_s/L is slow, happening only through $(pL/D)\log(\pi\,d_s/pL)$ as shown in equation (1).

The extreme case would be realized with n=1, p=N: the correspond-ing structure would have one stem per drift tube, with stems helically arranged in a superperiod NL. Such a structure, however, has no symmetry plane where to put the metallic end-plates closing the cavity. In order to keep a symmetry plane in the structure, the best choice is $p = 2$ because it avoids repeating the same stem arrangement in one superperiod.

With $p = 2$ we may take $n = N/2$ or $(N+1)/2$, according to which is an integer. Doing so, we transform the stem arrangements of figures 3a, 5b and 6b respectively into those of figures 8, 9, 10. Figure 9 and the three arrangements of figure 10, having the same angle $\emptyset$ and the same superperiod, are practically equivalent. It should be noticed that figure 10a when $\emptyset = \pi/2$ is nothing but the cross-bar structure. Finally, figure 11 shows the most efficient structure having three stems per drift tube.

5. CHOICE OF OPTIMUM STEM CONFIGURATION

As made clear in § 1, the optimum stem configuration and stem diameter are such that $\omega_b = \omega_a$. Representative points of the 0-mode frequency ω_a of typical Alvarez structures [9] are indicated in figure 4, for a proton energy range 1-200 MeV : they all fall between the curves $\nu = 1$ and $\nu = 3/2$ corresponding to $N = 2$ and $N = 3$. Since these curves represent an upper limit of ω_b for thick stems, it is obvious that at least a 3-stem pattern is needed. With a superperiod 2L, this leads to use two stems per drift tube, with the 3-stem configuration of fig. 9 or the more symmetrical 4-stem configurations of fig. 10. In what follows, we retain only the latter ones.

For comparison, the stem configurations which have been used so far in proton linacs are 1 stem (figure 2d) or 2 stems at 90° (figure 3a). Since the corresponding ν values are so low as 1/2 and 2/3 , ω_b is always much lower than ω_a . The stem passband is then so distant from the E_{01} passband that its influence on the latter is very small : with respect to the no-stem case, the effect on mode spacing around ω_a is almost negligible. The same argument would apply to multistem configurations, if the stems are thin enough. Nevertheless, for 2 stems at 180°, $\nu = 1$ and with practical stem diameters, ω_b may come rather close to ω_a (depending on the energy) : the influence of the stems on the E_{01} dispersion curve must then not be neglected (see later, curves 4 and 5 in figure 21).

RF losses on the stems being proportional to their diameter, thin stems would be desirable. But for mechanical reasons, a stem diameter of 2.5 cm at 200 MHz seems a minimum : we therefore restrict the practical stem diameters to the range 2.5 - 12.5 cm. Since the effect of d_s/L on ω_b appears only through $(pL/D)\log(\pi\, d_s/pL)$, it will be very small at low energies $(L/D \ll 1)$ while becoming more pronounced at high energies.

<u>Low energies (0.75 - 10 MeV)</u> $0.064 < L/D < 0.24$

Due to the smallness of L/D, it is impractical to adjust ω_b by varying d_s. Even with the smallest d_s (2.5 cm), $\pi\, d_s/2L$ ranges from 0.655 to 0.18, so that $(2L/D)\log(\pi\, d_s/2L)$ is indeed very small. This means that the upper limit of ω_b as given in figure 4 is a good approximation to ω_b : it is just needed to determine ν from the curve which passes through the representative point of the Alvarez structure. The relation $\emptyset = \pi/\nu$ yields the maximum angle $\emptyset$ between stems for anyone of the figure 10 - configurations.

According to equation (1), increasing L with constant d_s and D, lowers ω_b when $\emptyset$ is fixed. In order to keep ω_b at its optimum value ω_a, it is necessary to progressively decrease $\emptyset$, until at some energy around 10 MeV this angle reaches its minimum value $\pi/2$: the corresponding stem configuration is then the cross-bar structure (fig. 10a) or its equivalent (fig. 10b or 10c).

<u>Medium energies (10 - 30 MeV)</u> $0.24 < L/D < 0.41$

The cross-bar structure is adequate provided d_s is increased with energy. In order to compute the optimum value of d_s, we observe from figure 4 that the introduction of drift-tubes lowers both ω_a and ω_b. Assuming as a first approximation this effect to be about the same on both frequencies, we may derive the optimum d_s from a structure with stems but without drift-tubes. The problem is further simplified by considering a square guide with side D instead of the circular guide with diameter D. Then, as a first approximation [8], the condition for $\omega_b = \omega_a$ reads from equation (1) :

$$-\frac{pL}{D} \cdot \log\left(\pi\,\frac{d_s}{pL}\right) = \frac{8}{3\pi} \qquad \frac{pL}{D} \ll 1 \qquad (2)$$

This relation corresponds to $N = 4$ with
 $p = 1$: 4-stem structure (stems at 90°)
 $p = 2$: cross-bar structure.

When L/D increases, equation (2) becomes less accurate and must be replaced by the more exact conditions [8] :

for the cross-bar structure

$$-\log\left(\frac{\pi}{4}\,\frac{d_s}{D}\right) = \frac{2}{\pi\,\frac{L}{D}} + 1.944 - \pi\,\frac{L}{D} - \sum_{m=3,5\ldots}^{\infty} \frac{1}{\sqrt{m^2-1}}\,\frac{4}{e^{2\pi\sqrt{m^2-1}\cdot\frac{L}{D}}-1} \quad (3)$$

for the 4-stem structure

$$-\log\left(\frac{\pi}{4}\,\frac{d_s}{D}\right) = \frac{4}{\pi\,\frac{L}{D}} + 1.419 - \sum_{m=3,5\ldots}^{\infty} \frac{\sqrt{m^2-1}}{m^2-4}\,\frac{4}{e^{\pi\sqrt{m^2-1}\cdot\frac{L}{D}}-1} \quad (4)$$

In both cases the group velocity at the crossing point of the dispersion curves is approximately given by

$$\frac{v_g}{c} \approx \frac{1}{2\sqrt{2}} = 0.354 \qquad (5)$$

The relations (3) and (4) have been plotted in figure 12.

For the cross-bar structure
at 10 MeV, $L/D = 0.24$, equation (3) gives $d_s = 2.5$cm ($L = 22$cm)
at 30 MeV, $L/D = 0.41$, equation (3) gives $d_s = 12.6$cm ($L = 37$cm)

For the 4-stem structure
at 10 MeV, $L/D = 0.24$, equation (4) gives $d_s = 0.2$cm ($L = 22$cm)
at 30 MeV, $L/D = 0.41$, equation (4) gives $d_s = 1.3$cm ($L = 37$cm)

The cross-bar structure thus leads to practical stem diameters up to 30 MeV. The 4-stem structure, being more efficient, would require too thin stems in this energy range (see fig. 12).

<u>Medium energies (30 - 50 MeV)</u> $0.41 < L/D < 0.52$

It is now necessary to use at least $n = 3$ stems per drift-tube, and this number is enough, because for the 4-stem structure at 50 MeV, equation (4) gives $d_s = 2.4$ cm. The 3-stem structure of fig. 13

will therefore need stem diameters larger than 1.3 - 2.4 cm, but smaller than $L/\pi = 11.8 - 15.0$ cm (the latter values would put ω_b on the $\nu = 3/2$ curve in fig. 4) : it is thus adequate in the energy range 30 - 50 MeV.

<u>High energies (50 - 200 MeV)</u> $0.52 < L/D < 1.01$

For the 4-stem structure at
50 MeV, $L/D = 0.52$, equation (4) gives $d_s = 2.4$cm ($L = 47$cm)
100 MeV, $L/D = 0.75$, equation (4) gives $d_s = 4.8$cm ($L = 64$cm)
200 MeV, $L/D = 1.01$, equation (4) gives $d_s = 7.3$cm ($L = 85$cm).

The 4-stem structure of fig. 14 is thus adequate. Another possibility is the 6-stem configuration of fig. 11, with three stems per drift tube and superperiod 2L.

6. EXPERIMENTAL RESULTS

Extensive measurements of dispersion curves have been carried out with two scale models of linac tanks. Although the variations of Alvarez cells with energy were carefully reproduced on the models, no attempt has been made to close the stopband locally along the full length of the tank: this indeed would involve varying the stem angle or the stem diameter from drift-tube to drift-tube. In a final design, it should be done at least from one small group of drift-tubes to the next. In our models, both the stem angle and the stem diameter were kept constant throughout the tank : by virtue of equation (1), this results in a decrease of the local ω_b from the low energy end to the high energy end of the tank.

The corresponding local dispersion curves are shown in fig. 15 : when frequency approaches the zero-mode of the bar resonances, the tank is progressively cut off, starting from the long cell end in the undercompensated case, and from the short cell end in the overcompensated case. In the vicinity of ω_b, the phase shift per cell θ is thus no longer precisely defined, and this explains why the experimental dispersion curves show some irregularities in this frequency region. The same argument applies to the π-mode cut-off regions. Near ω_a, a tank compensated on the average is partially cut off at the long cell end when $\omega < \omega_a$, and at the short cell end when $\omega > \omega_a$ (fig.15 c).

In all measurements the modes were identified by a bead perturbation technique. Figure 16 shows the measured variation of E_z^2 along a tank partially cut off (modes close to the 0 or π-end of the stem passband). The zeros of the field become more widely spaced towards the cut-off region, where the field decays to the end plate without passing through another zero. Near the end of the tank which is cut off, there results a long region without field zeros, that progressively shrinks as a greater length of the tank propagates.

As a check of the basic principles used in §3 and 4, fig. 17 shows a comparison between the theoretical upper limit of ω_b deduced from fig. 4, and the experimental value extrapolated from the measured dispersion curves for various stem configurations. The general trend of ω_b is as expected from the theory.

When applying the theory to our variable cell models, we simply used the arithmetic mean value of L, which is also very close to the length of the middle cell.

Tank 1 model (0.75 - 5 MeV)

With a reduction factor 0.190, this model is scaled from the first 25 cells of the new 20 MeV linac injector for the 3 GeV proton synchrotron SATURNE in Saclay. The stem diameter, although having the smallest practical value of 2.5 cm at 200 MHz, still gives a $\pi\, d_s/\langle L\rangle$ as large as 0.754. The upper limit of $\emptyset$, derived as in § 5, should thus be only slightly in excess of the correct value. In fact, the theoretical limit is 143°, whereas the optimum experimental value is about 135° : this is clear from fig. 18, which shows the dispersion curves corresponding to several stem angles $\emptyset$.

At 0-mode, the measured group velocity for the compensated structure is 0.394 c.

Tank 2 model (10 - 30 MeV)

With a reduction factor 0.162, this model is scaled from the actual 41-cell tank 2 of the CERN 50 MeV linac injector, which is identical with the PLA Tank 2 in the Rutherford High Energy Laboratory. Since $\langle L\rangle/D = 0.3145$, the optimum structure is the cross-bar with $d_s = 9.71$ mm (model value). For the 4-stem structure, equation (4) yields $d_s = 0.94$ mm.

In order to check these theoretical values, measurements have been made with $d_s = 1.0$ mm, 6.16 mm (scaled from the actual value at 202.5 MHz) and 12.0 mm, using many different stem configurations. The most interesting results have been selected in figs. 19 and 20. It is seen that the presented theory fits well all experimental data.

The main difference occurs for the optimum stem diameter of the 4-stem structure: the structure with $d_s = 1.0$ mm appears to be slightly under-compensated, whereas theoretically it should be overcompensated.

At 0-mode, the experimental group velocity is estimated to be about 0.39 c for the compensated cross-bar structure, and 0.37 c for the compensated 4-stem structure. These figures compare favourably with the theoretical estimate (5).

Tank 2 model has also been used to verify that the presence of either one stem per drift tube or two stems at 90°, has only a small influence on the E_{01} passband. The first few modes of this pass-band are plotted in fig. 21 for six different stem configurations with $d_s = 6.16$ mm. The stem configurations which yield the smallest mode spacing around ω_a are No. 1 (one stem per drift tube) and No. 2, 3 (two stems at 90°). The stem configuration No. 1 has also been measured with $d_s = 1$ mm: the corresponding dispersion curve is shifted down by about 2 MHz with respect to the case $d_s = 6.16$ mm.

The main effect of the stems in these configurations is to shift ω_a and the neighbouring modes slightly up in frequency, by an amount which may be computed for thin stems with Slater's perturbation formula.

Finally, it should be observed that configuration No. 1 has a larger mode spacing than configurations No. 2 and 3, despite the fact that ω_b is higher for the latter ones. The probable explanation is that although the influence of the stem passband on the E_{01} passband is mainly determined by the difference $(\omega_a^2 - \omega_b^2)$, the shape of the E_{01} passband also depends on the coupling between stems and/or between stems and drift-tubes.

Uniform 100 MeV models (Brookhaven, Los Alamos)

In the energy range 50 – 200 MeV, the 4-stem structure is adequate. On his 6 cell, 100 MeV model [6], Giordano closed the stopband by putting 1.905 cm flares on the stems (he used $d_s = 0.635$ cm), whereas equation (4) predicts an optimum stem diameter of 1.15 cm. Similarly, Los Alamos measurements on a 10 cell, 92.7 MeV model [10] show the stem diameter to be about 2.016 cm for closed stopband, whereas the computed value is 1.75 cm.

The experimental group velocity at 0-mode is 0.322 c for the Brookhaven model, and 0.352 c for the Los Alamos model.

7. CONCLUSION

The presented theory, although approximate, enables one to choose from all multistem structures the stem configuration that, with a practical stem diameter, suppresses the stopband at the operat-ing E_{010} mode for any proton energy in the range 0.75 – 200 MeV.

Instead of stems, other couplers may be used to produce a second passband which is adjusted to cross the E_{01} passband at 0-mode. For example, alternating T-bar and post couplers have recently been investi-gated in Los Alamos on a 10 cell, 92.7 MeV model [10] . These couplers are easier to tune and present less RF losses than 4 stems. Neverthe-less, due to a smaller coupling with the drift-tubes, they produce a smaller group velocity at 0-mode in a compensated structure: this group velocity is of the order of 0.12 c, compared with 0.354 c for a compen-sated 4-stem structure.

Finally, it should be remembered [5] that for energies above 100 MeV, the cross-bar structure operated in the $\pi/2$ mode of the stem-passband, features large mode spacing with a higher shunt impedance than the Alvarez structure. (This mode is called π mode in ref.5.)

REFERENCES

1. D.E. Nagle, E.A. Knapp, and B.C. Knapp: "A coupled resonator model for standing wave accelerator tanks", to be published in Rev. Sci. Instruments.

2. K. Batchelor, T. Nishikawa, and T. Werntz: "Numerical analysis of the RF field in a drift tube loaded cavity", Proceedings of the U.S. National Particle Accelerators Conference, Washington, March 1967 (IEEE Transactions on nuclear science, Vol. NS-14,

No.3, June 1967), p. 295.

3. R.M. Bevensee: "Electromagnetic slow wave systems", J. Wiley and Sons, New York, 1964, Chapter V, 5-5 and 5-6.

4. P.D. Dunn, C.S. Sabel and D.J. Thompson: "Coupling of resonant cavities by resonant coupling devices", AERE Report GP/R 1966, December 1956.

5. A. Carne, G. Dôme, N. Fewell, W. Jüngst: "Development of the cross-bar structure for a proton linear accelerator", Proceedings of the V International Conference on High Energy Accelerators, Frascati, September 1965 (CNEN, Rome, 1966), p. 624.

6. S. Giordano and J.P. Hannwacker: "Measurements on a multistem drift tube structure", Proceedings of the 1966 Linear Accelerator Conference , Los Alamos, October 1966, LA-3609 (CFSTI, Springfield, Virginia), p. 88.

7. S. Giordano: "A new multistem, drift-tube, standing wave, zero-mode proton accelerating structure", Brookhaven National Laboratory Accelerator Dept. Internal Report AGSCD-7, February 1966.

8. G. Dôme: "Rod loaded waveguides", to be published.

9. MURA linac cavity calculations, 0.75 – 200 MeV, March 1967.

10. E.A. Knapp, J.M. Potter, E.J. Schneider, and D.A. Swenson: "Stabilization of the drift tube linac by operation in the $\pi/2$ cavity mode", Los Alamos Scientific Laboratory Internal Report MP-3/EAK/JMP/EJS/DAS-1, June 1967 (Private communication).
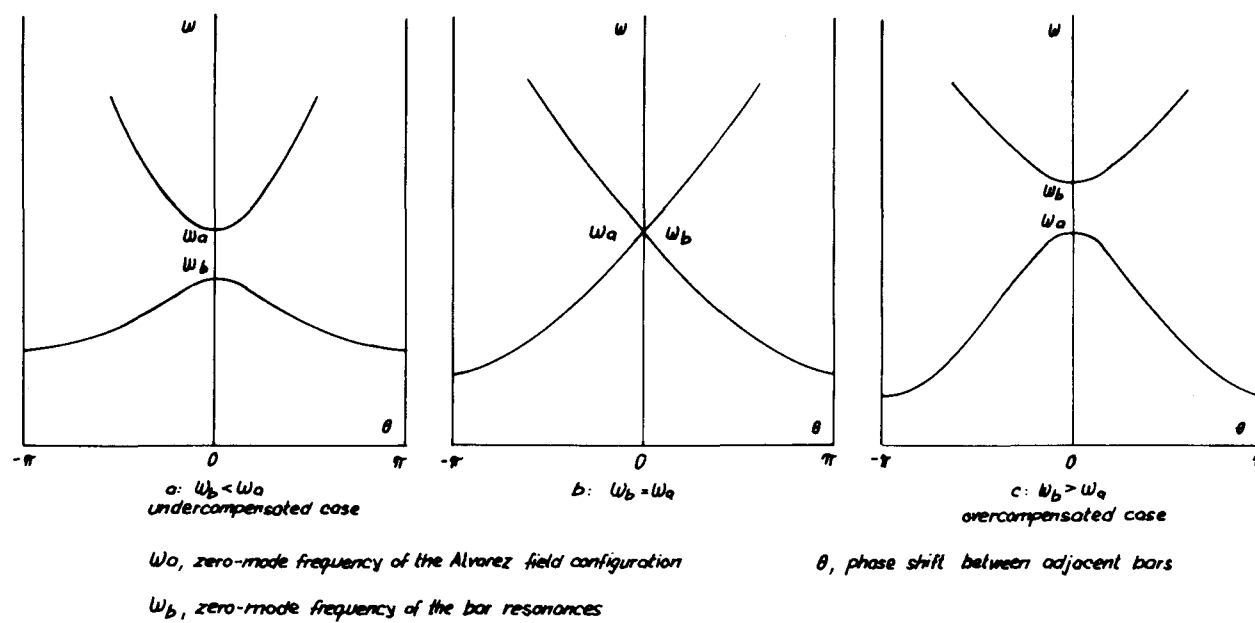
a: $\omega_b < \omega_a$
undercompensated case

b: $\omega_b = \omega_a$

c: $\omega_b > \omega_a$
overcompensated case

ω_a, zero-mode frequency of the Alvarez field configuration

θ, phase shift between adjacent bars

ω_b, zero-mode frequency of the bar resonances

Figure 1. Dispersion curves of the E_{01} and bar passbands.
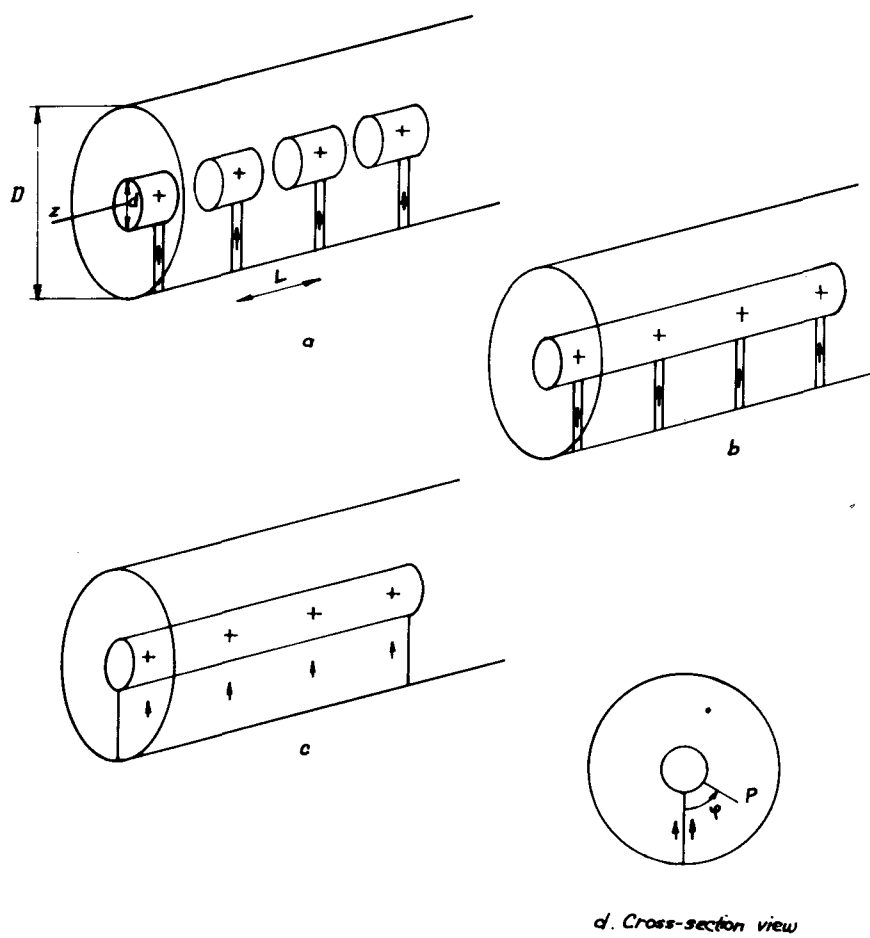(The bar diameter is increasing from a to c).

d. Cross-section view

Figure 2.   Successive transformations of a structure with short
cells of 0-mode.
↕ Conduction current

$\pi \leq \phi \leq 2\pi$

a

b

$\nu \frac{\phi}{\pi} = 1,3,5,.....$

$\nu \frac{\phi}{\pi} = 0,2,4,.....$
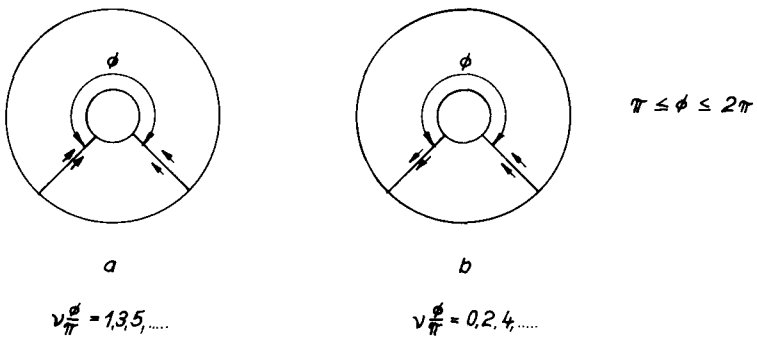
Figure 3. Two stems per drift tube

$\frac{2\pi}{3} \leq \phi \leq \pi$

$\nu \frac{\phi}{\pi} = 1 \; : \; 1 \leq \nu \leq \frac{3}{2}$

a

b
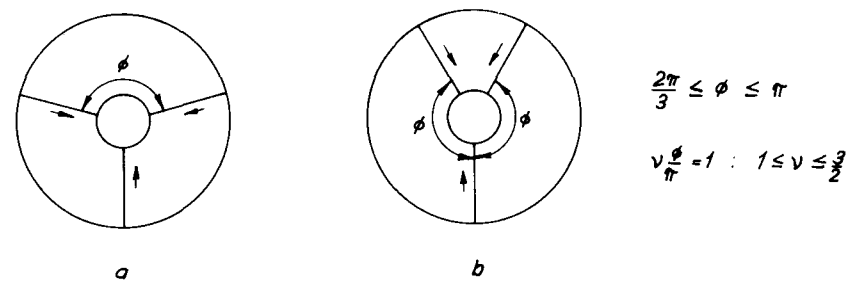
Figure 5. Three stems per drift tube
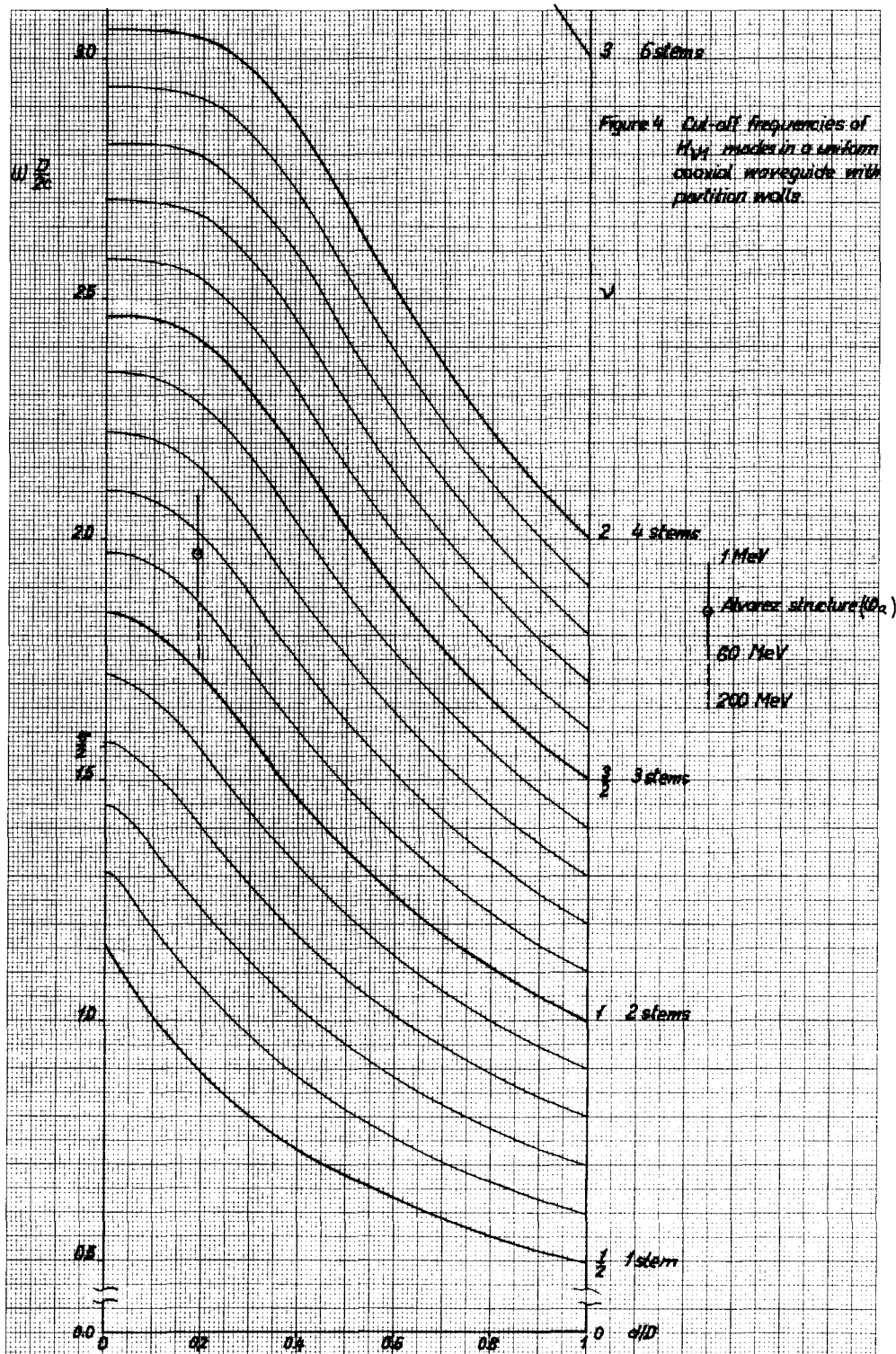
Figure 4. Cut-off frequencies of
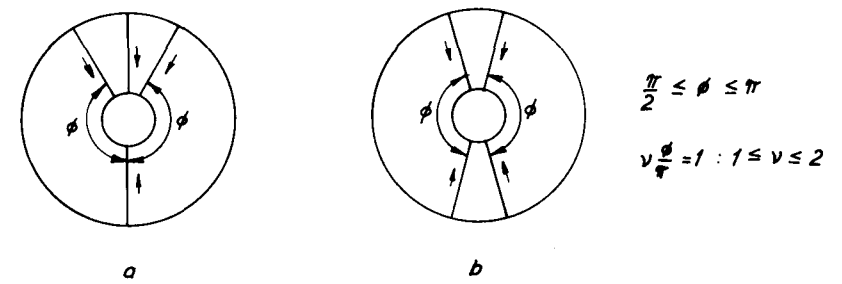$H_{\nu\nu}$ modes in a uniform
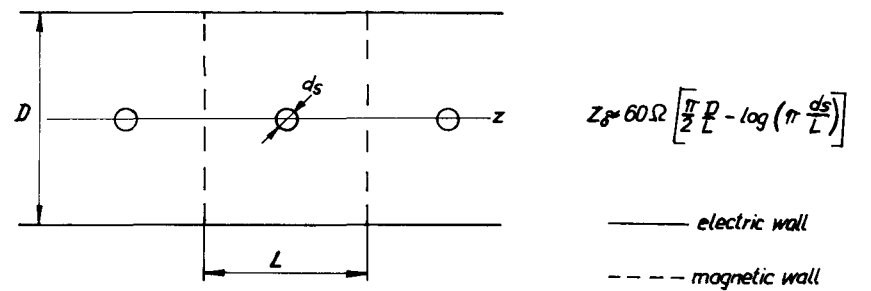coaxial waveguide with
partition walls.

6 stems

4 stems

1 MeV

Alvarez structure (ω_0)

60 MeV

200 MeV

3 stems

2 stems

1 stem

$\frac{\pi}{2} \leq \phi \leq \pi$

$\nu \frac{\phi}{\pi} = 1 \; : \; 1 \leq \nu \leq 2$

a

b

Figure 6. Four stems per drift tube

$Z_s \approx 60\,\Omega \left[\frac{\pi}{2} \frac{D}{L} - \log\left(\pi \frac{d_s}{L} \right) \right]$

———— electric wall

– – – – magnetic wall

Figure 7. Cross-section of the stem transmission line
in O-mode

$\pi \leq \phi \leq 2\pi \quad \frac{1}{2} \leq \nu \leq 1$

Figure 8. N=2, n=1

$\frac{2\pi}{3} \leq \phi \leq \pi \quad 1 \leq \nu \leq \frac{3}{2}$
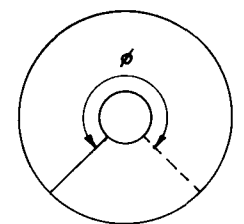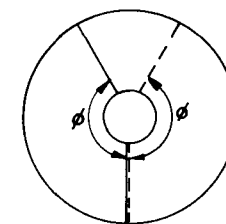
Figure 9. N=3, n=2

Figure 10. N=4, n=2

Figure 11. N=6, n=3

Figure 13. N=3, n=3
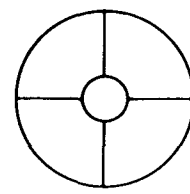
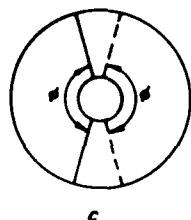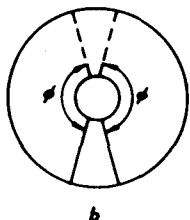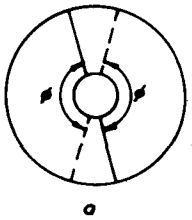Figure 14. N=4, n=4

$\frac{\pi}{2} \leq \phi \leq \pi$

$1 \leq \nu \leq 2$

——— Stems on even drift tubes

— — — Stems on odd drift tubes

N-stem configurations with superperiod 2L.
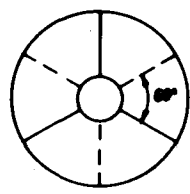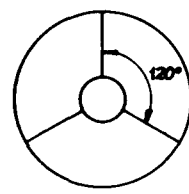
n, number of stems per drift tube
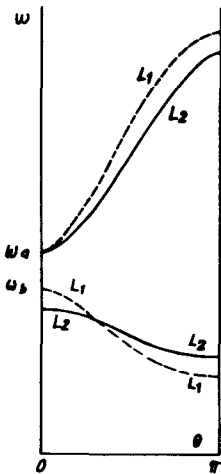

undercompensated for L_1, L_2
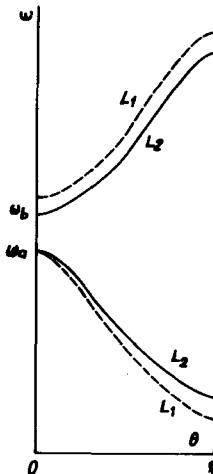
overcompensated for L_1, L_2
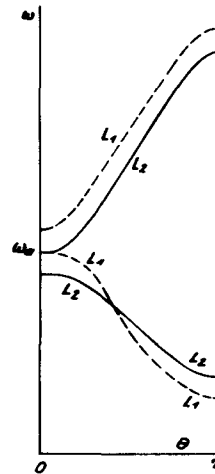
overcompensated for L_1
undercompensated for L_2

a

b

c

Figure 15. Dispersion curves for variable L structures $(L_1 < L_2)$
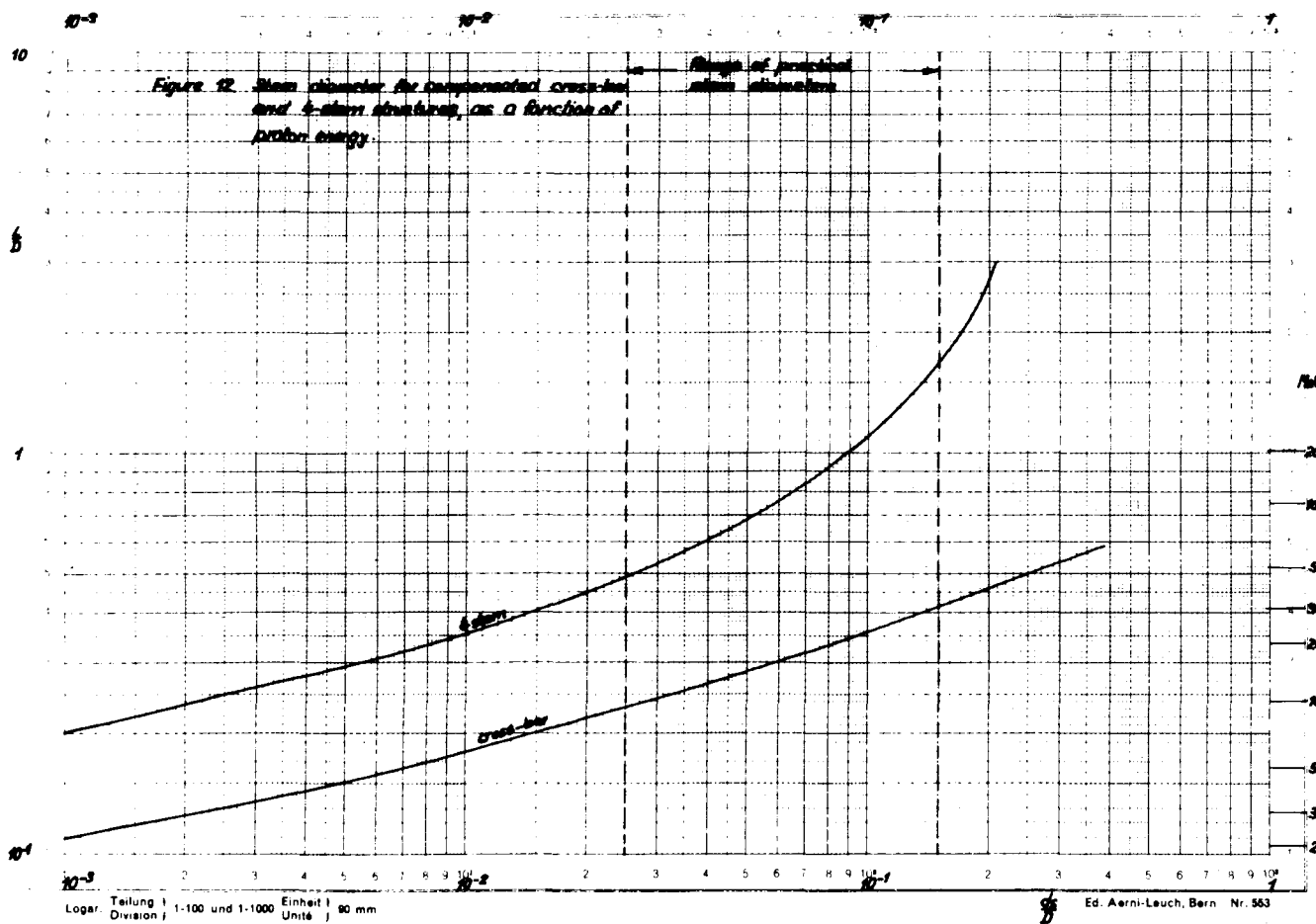
Figure 12. Stem diameter for compensated cross-bar and 6-stem structures, as a function of proton energy.

A-26

Figure 16. Variation of E_z^2 along tank 2-model (41 cells), showing partial cut-off near 0-mode. Part 1.

Figure 16. Variation of E_z^2 along tank 2-model (41 cells), showing partial cut-off near 0-mode. Part 2.

TANK 1-MODEL

THEORETICAL UPPER LIMIT (MHz)

EXTRAPOLATED EXPERIMENTAL VALUES (MHz)

$D = 190$ mm
$<d> = 33.86$ mm
$<L> = 19.79$ mm
$d_s = 5.0$ mm

462	480	
605	640	
868	880	860 / 880
1215	1190	1170 / 1130
1527	1470	1260 / 1240

TANK 2-MODEL

$D = 150$ mm
$d = 28.77$ mm
$<L> = 47.19$ mm
d_s in mm

576 — $d_s = 12.0$ 590 / $d_s = 6.16$ 550

756 — $d_s = 12.0$ 800 / $d_s = 6.16$ 750 ; $d_s = 12.0$ 710 / $d_s = 6.16$ 670
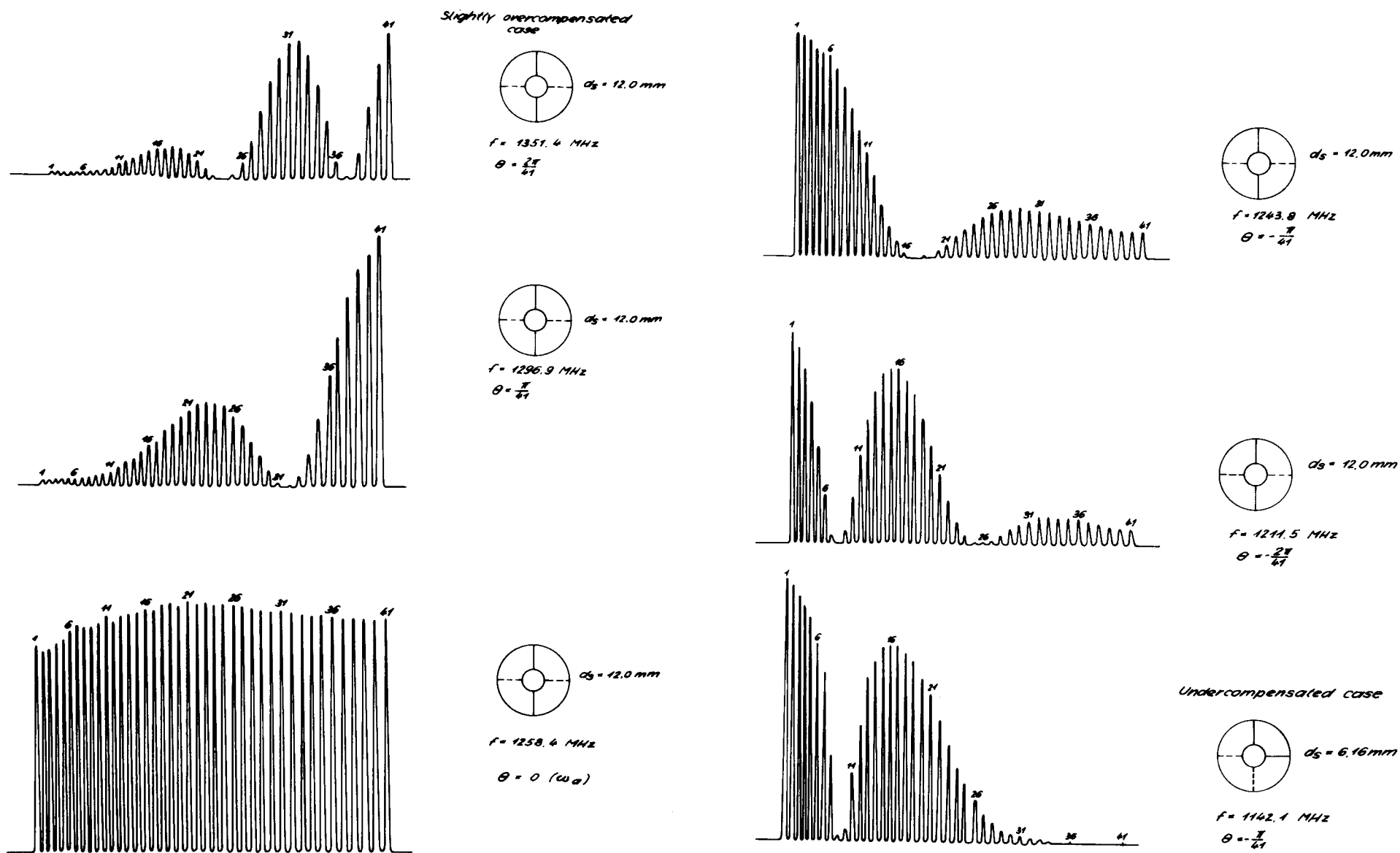
— Stems on even drift tubes
---- Stems on odd drift tubes

1090 — $d_s = 12.0$ 1080 / $d_s = 6.16$ 1000 ; $d_s = 12.0$ 900 / $d_s = 6.16$ 800

1931 — $d_s = 12.0$ 1740 / $d_s = 6.16$ 1450 / $d_s = 1.0$ 1200 ; $d_s = 12.0$ 1250 / $d_s = 6.16$ 1210 ; $d_s = 12.0$ 1260 / $d_s = 6.16$ 1200 / $d_s = 1.0$ 960
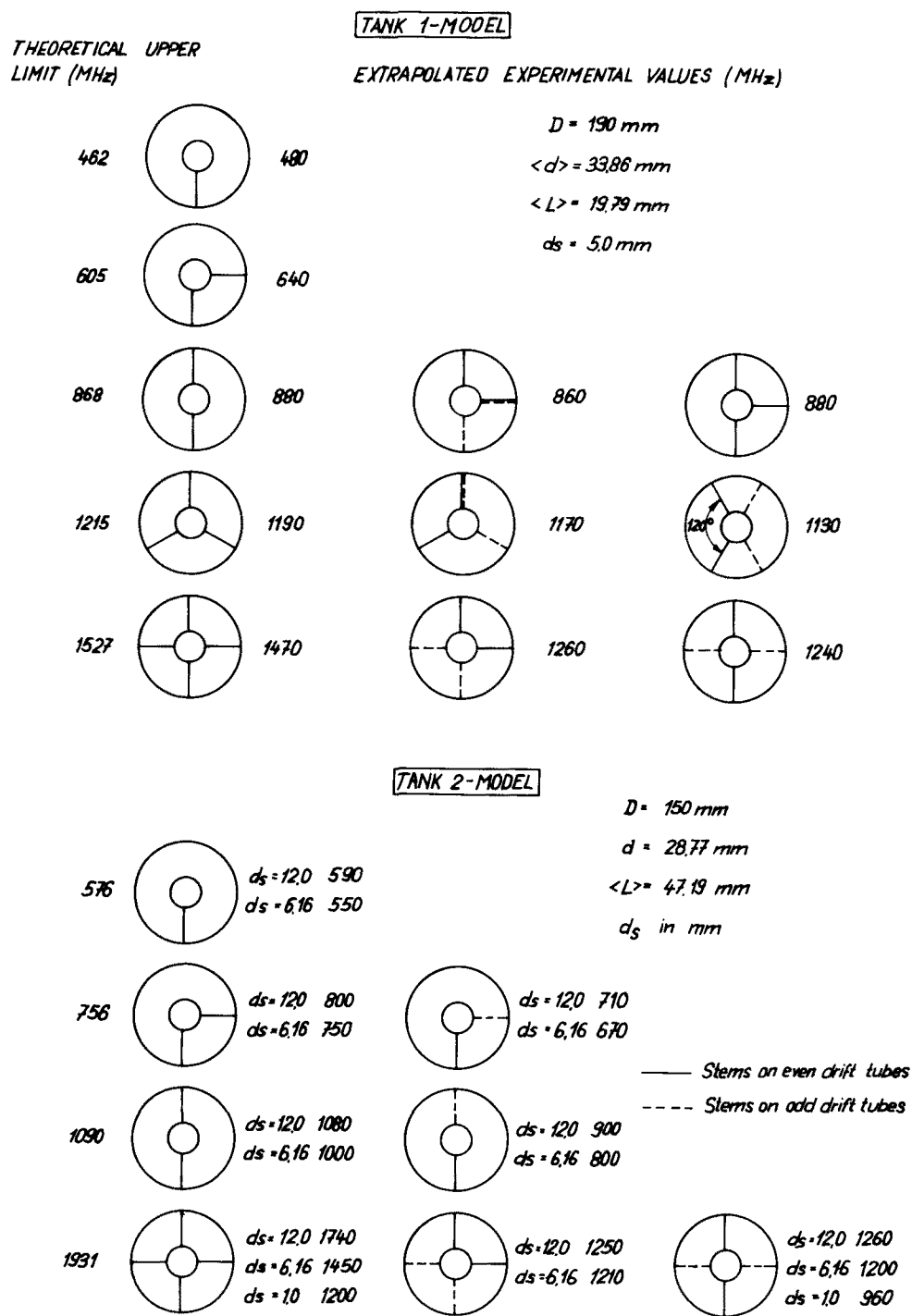
Figure 17. COMPARISON OF THEORETICAL AND EXPERIMENTAL VALUES OF f_b FOR VARIOUS STEM CONFIGURATIONS

Figure 18. Dispersion curves of tank 1-model for several stem angles φ.

For a compensated structure, $\frac{v_g}{c} = 0.394$ at 0-mode

Figure 19. Dispersion curves of tank 2-model with cross-bar structure

For a compensated structure,
$\frac{v_g}{v} \approx 0.39$ at 0-mode

Figure 20. Dispersion curves of tank 2-model with 4-stem structure

For a compensated structure,
$\frac{v_g}{v} \approx 0.37$ at 0-mode

Figure 21. The first modes of the E₀₁ passband in tank 2 model for various stem configurations.